Journal of Materials Chemistry A

PAPER

View Article Online
View Journal | View Issue

Cite this: J. Mater. Chem. A, 2017, 5, 21486

Half-metallic TiF_3: a potential anode material for Li-ion spin batteries

Junru Wang,[a] Feng Li,[ab] Bo Yang,[a] Xiaobiao Liu[a] and Mingwen Zhao *[a]

Received 11th August 2017
Accepted 17th September 2017

DOI: 10.1039/c7ta07092f

rsc.li/materials-a

As a key component of spintronic devices, spin batteries that can generate spin-polarized current are drawing increasing interests. Herein, we propose a simple strategy for spin batteries by introducing a half-metallic anode material in the conventional Li-ion batteries. Using first-principles calculations, we demonstrate a potential half-metallic anode material, TiF_3 crystal, which has stable ferromagnetism and half-metallicity under Li insertion. Low Li diffusion barriers (0.16–0.37 eV) and moderate Li storage capacity (256 mA h g^{-1}) are revealed in the TiF_3 crystal. The combination of half-metals and Li-ion battery offers a new solution for spin batteries.

Introduction

As an indispensable part of the modern society, high performance rechargeable batteries, *e.g.* lithium-ion batteries (LIBs), are drawing increasing interests.[1,2] LIBs are composed of a cathode, an anode and the electrolyte between them. Electrode materials are quite crucial for the properties of LIBs, such as life cycle, storage capacity, and charging/discharging rates. Compared with cathodes, the development of the anode materials has not been satisfactory to date; *i.e.* the performance of LIBs is largely determined by the anode materials.[3–6] Ideal anode materials should have good conductivity, low Li diffusion barriers, high storage capacity, high stability, *etc.* Numerous materials have been proposed as promising anode materials with good performance, such as graphene and related systems,[7–9] transition-metal dichalcogenides (MoS_2),[10] transition-metal carbides (Ti_3C_2),[11] metal nitrides,[12] MXenes,[13] phosphorene[14] and so on.[15,16] Notably, all known anode materials are nonmagnetic, where the electron spin effects are not included.

Spintronics, based on the manipulation of the intrinsic spin of electrons and its associated magnetic moments in addition to its fundamental electron charge, has been a long standing subject since the 1980s[17–19] due to its promising applications such as information storage, transportation and processing. Half-metals, a class of materials that behave as a metal in one spin direction and an insulator in the opposite spin direction, are ideal for spintronics applications, as it can filter the current into a single spin channel. To this day, a number of materials with half-metallicity have been proposed, such as chromium dioxide,[20] transition metal doped dilute magnetic semiconductors,[21] sp half-metallic ferromagnets,[22–25] Heusler compounds,[17,26–29] and magnetic perovskites.[30] However, none of them is implementable for the anode of Li-ion batteries because the intrinsic voids in these materials are not large enough to host Li ions. The only exception is CrO_2,[20] but the half-metallicity is lost after Li intercalation.

An interesting question naturally arises: are there half-metallic anode materials suitable for LIBs? If a half-metallic anode is introduced into LIBs, the spin-filter ability of half-metals may offer a promising solution for the long-desired spin batteries. In this study, on the basis of first-principles calculations, we propose for the first time a potential half-metallic anode material, TiF_3 crystal, which has been synthesized in experiments.[31,32] We demonstrated that the TiF_3 crystal has robust ferromagnetism and half-metallicity under Li insertion. The diffusion barrier of Li ions in the TiF_3 crystal is about 0.16–0.37 eV, implying the high Li mobility and thus high charging/discharging rates. The Li storage capacity in the TiF_3 crystal is about 256 mA h g^{-1}, comparable to that of most of the LIBs. Because the TiF_3 crystal represents a large family of materials,[33–35] it is expected that the present findings can shed light on a new way to develop LIBs involving electron spin-polarization.

Computational methods

Our first-principles calculations were performed within the framework of density-functional theory (DFT), which is implemented in the Vienna *ab initio* simulation package known as VASP.[36] The electron–ion interactions were described by projector-augmented-wave (PAW) potentials.[37] The generalized gradient approximation (GGA) in the form of Perdew–Burke–Ernzerhof (PBE) was adopted for the exchange–correlation functional.[38,39] The plane waves employed to expand the Kohn–

[a]School of Physics, State Key Laboratory of Crystal Materials, Shandong University, Jinan 250100, Shandong, China. E-mail: zmw@sdu.edu.cn
[b]School of Physics and Technology, University of Jinan, Jinan 250022, Shandong, China

Sham electron wavefunction have an energy cutoff of 520 eV. Structural optimizations were carried out using a conjugate gradient (CG) method without any symmetry until the maximum force on each atom was less than 0.01 eV $Å^{-1}$. The TiF_3 crystal was modeled using a $2 \times 2 \times 2$ supercell repeated periodically along the *x*-, *y*-, and *z*-directions. The Brillouin zone (BZ) integration was sampled on a $9 \times 9 \times 9$ *k*-point grid.[40] For the TiF_3 nanosheet, a vacuum region of 20 Å was along the *z*-directions to avoid the interactions between neighboring images. In the spin-polarization calculations, different initial spin configurations were adopted to get the magnetic moment of the ground state. Electron spin-polarization was taken into account throughout the calculations. The energetic minimal path profiles for the Li diffusion were determined using a nudged elastic band (NEB) method.[41,42]

Results and discussion

A. Half-metallicity of ferromagnetic TiF_3 crystal

TiF_3 crystal has a cubic lattice with a space group of $pm\bar{3}m$. Ti atoms reside in the corners of the cubic lattice, while F atoms are at the edge centers, as shown in Fig. 1(a). Each Ti atom bonds to six F atoms, while each F atom is coordinated by two Ti atoms. The lattice constant, which is twice the Ti–F bond length, is about 3.933 Å. The large voids in the center of the cubic lattice facilitate the accommodation and diffusion of small-size ions like lithium.[33,43–45]

The electronic band structure of the TiF_3 crystal was then calculated. It is found that the TiF_3 crystal has a spin-polarized ground state with significant spin-splitting of about 1.0 eV, as shown in Fig. 1(b). The half-metallicity of the TiF_3 crystal is quite evident. The Fermi level crosses the bands of one spin channel, leading to abundant electronic states at the Fermi level, whereas a large band gap of about 5.478 eV appears in the opposite spin channel. The bands in the proximity of the Fermi level are rather dispersive in the momentum space, suggesting good conductivity of the conducting spin channel.

We also employed a large supercell ($2 \times 2 \times 2$) to investigate the possible spin configurations of the TiF_3 crystal. Starting from different initial spin configurations, self-consistent calculations give six types of magnetic orderings, as shown in Fig. 2(a). It is found that the ferromagnetic (FM) ordering is energetically the most favorable. The energies of the five antiferromagnetic (AFM) orderings relative to the FM ordering are listed in Fig. 2(a). The smallest energy difference (ΔE) between FM and AFM is about −30 meV per unit cell. The FM state has magnetic moments of 1 μ_B in one unit cell, residing at the Ti ions. This is reasonable because the Ti atom in the TiF_3 crystal is at the +3 state with one unpaired electron in each Ti.

The origins of the electron spin-polarization were revealed from the electron density of states (DOS) analysis. Fig. 2(b) and(c) gives the total DOS (TDOS) and the DOS projected onto different atomic orbitals (PDOS) of the ferromagnetic TiF_3 crystal. The half-metallicity of the TiF_3 crystal is quite obvious from the TDOS. The abundant electronic states of one spin channel in the proximity of the Fermi level arise mainly from the d_{xy}, d_{yz} and d_{xz} orbitals of Ti ions with a small contribution from the p orbital of F. This is in good consistency with the symmetry of the TiF_3 crystal. The Ti^{3+} ion resides in the center of the octahedron of the nearest F atoms. According to the crystal field theory, the five d orbitals of Ti^{3+} ion in a octahedral crystal field split into a three-fold degenerate e_g orbital (d_{xy}, d_{yz} and d_{xz}) and doubly-degenerate t_{2g} (d_{z2} and d_{z2-y2}) orbital. The e_g orbital is lower in energy than t_{2g}. Therefore, the unpaired electron in Ti^{3+} occupies the three-fold degenerated e_g and contributes magnetic moments of 1 μ_B. The overlap between Ti_e_g and F_p orbitals facilitates the p–d hybridization as well as the super-exchange between Ti^{3+} ions.

The energetic favorability of the FM ordering in the TiF_3 crystal can be interpreted in terms of a super-exchange mechanism,[46–48] as elucidated in Fig. 2(e). The three-fold degenerate e_g orbital of Ti^{3+} ion doesn't reach the half of electron

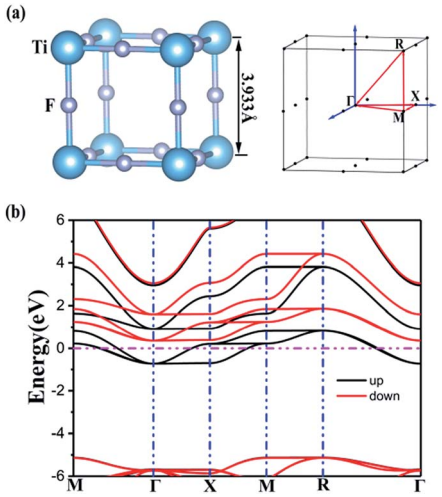

Fig. 1 (a) Unit cell (left) and Brillouin zone (right) of the TiF_3 crystal. Ti and F atoms are represented by the large and small balls, respectively. The highly symmetric points are marked. (b) Electronic band structure of the TiF_3 crystal. The energy at the Fermi level was set to zero.

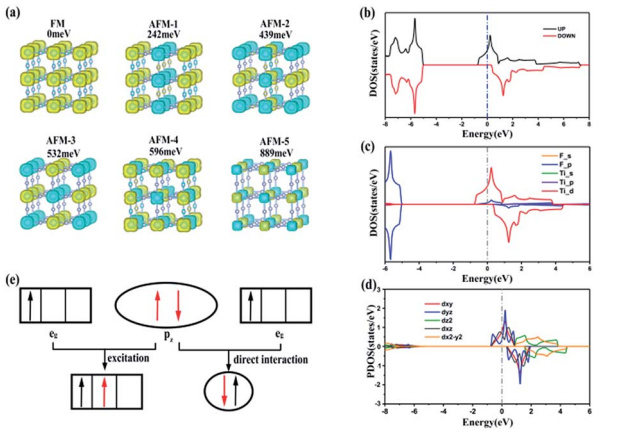

Fig. 2 (a) Electronic of density of states (DOS) of TiF_3. (b) The partial density of states (PDOS) of TiF_3. (c) Spin-resolved electron density of the d orbitals of TiF_3. (d) The spin-polarized electron density for FM and AFM; the isovalue is 0.004 e $Å^{-3}$. (e) Schematic diagram of the energetic favorability of the FM ordering in the TiF_3 crystal.

occupation, while the F^- ion connecting two Ti^{3+} ions has a closed 2p shell. According to the Goodenough–Kanamori rules,[46–48] the F^- with closed 2p shell mediates a FM ordering of the Ti^{3+} ions, which is confirmed by our first-principles calculations.

B. The half-metallicity and ferromagnetism of TiF_3 under Li insertion

For a potential anode material for LIBs, the electronic structure modification in response to Li insertion, particularly the stability of the half-metallicity, is quite crucial. We investigated the electronic structures of TiF_3 with different Li concentrations. We first placed a single Li atom in a $2 \times 2 \times 2$ supercell of TiF_3, corresponding to a stoichiometry of $Li_{0.125}TiF_3$. Structural optimization showed that the inserted Li atom prefers the center of the F^- square on the {001} planes, as shown in Fig. 3(a), rather than the cubic center. The energy difference between the two sites is −48.5 meV per unit cell. This is related to the coulomb attraction between Li^+ and F^- ions. The formation energy of $Li_{0.125}TiF_3$ determined by the difference between the total energy of $Li_{0.125}TiF_3$, and the sum of the total energies of TiF_3 and bulk Li crystal is about −0.995 eV per Li. The negative formation energy indicates that the Li atom prefers to insert into TiF_3 rather than clustering. Bader analysis shows that about 0.87 electrons transfer from Li atom to TiF_3.

The spin-resolved DOS of the TiF_3 crystal at this Li concentration is plotted in Fig. 3(a). It is evident that the half-metallicity remains intact under Li insertion. We also calculated the energy difference between FM and AFM ordering and found that it is enhanced to −72 meV per unit cell, implying that the stability of ferromagnetism of the TiF_3 crystal is improved by Li insertion.

As the Li concentration is increased to $LiTiF_3$, corresponding to eight Li ions in a $2 \times 2 \times 2$ supercell, more electrons transfer to the TiF_3 crystal, pushing the Fermi level upwards to the conduction band region of the semiconducting channel, as shown in Fig. 3(b). However, highly-spin-polarized current could also be expected because the electronic states near the Fermi level arise mainly from the conductive spin channel. The FM ordering remains energetically most favorable, but the energy difference between FM and AFM ordering decreases to −41 meV per unit cell.

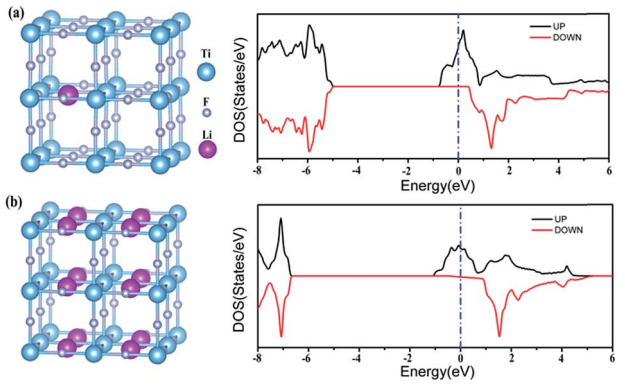

Fig. 3 The atomic structure and spin-resolved electron density of states (DOS) of (a) $Li_{0.125}TiF_3$ and (b) $LiTiF_3$. The energy at the Fermi level was set to zero.

C. Li diffusion barriers and storage capacity

The diffusion energy profile of a Li atom between two steady states (face centers) was determined using the CNEB strategy. For $Li_{0.125}TiF_3$, the energy barrier was calculated to be about 0.37 eV with the transition state (TS) residing at the Ti cubic center. When the Li concentration increases to $Li_{0.875}TiF_3$, corresponding to seven Li ions in a $2 \times 2 \times 2$ supercell, the potential barrier decreases to only 0.16 eV. The face center in this case is still the energy minimum site. The Li diffusion barriers in TiF_3 are much lower than those in silicon (0.57 eV)[49] and phosphorene categories (0.76 eV)[50] and comparable to that in graphene (0.33 eV),[8] implying high Li mobility and thus high charging/discharging rates.

We also evaluated the energy barrier of intercalating a Li atom from the surface to the interiors of TiF_3 using a slab model of a TiF_3 nanosheet. The energetically most preferable site for Li atom on the TiF_3 nanosheet remains to be the face center. As the Li atom enters the interiors of the TiF_3 nanosheet from the surface, it should experience an energy barrier of 0.37 eV. Such a low energy barrier implies that Li atom is easy to enter the interior of TiF_3. The energy barrier is lower than that of Cu_3N (0.81 eV).[33] From the interior of TiF_3 to the surface, however, Li ion should overcome an energy barrier of 0.48 eV as the interior face center is more stable than the surface face center by about 0.11 eV. This indicates that Li ion prefers to stay in the interior of TiF_3 rather than on the surface.

Li storage capacity and the average open-circuit of bulk TiF_3 are two key parameters that determine the performance of LIBs. The Li storage capacity can be evaluated from the formation energy (E_{form}) of the Li_xTiF_3 defined as $E_{form} = E_{Li_xTiF_3} - E_{TiF_3} - xE_{Li}$, where $E_{Li_xTiF_3}$ and E_{TiF_3} represent the total energy of TiF_3 with and without Li insertion, respectively, and E_{Li} is the energy of a Li in bulk crystal. When 8 Li atoms are placed in the cubic centers of a $2 \times 2 \times 2$ supercell, corresponding to a stoichiometry of $LiTiF_3$, the formation energy is about −0.08 eV per Li. According to the definition of the formation energy, the negative formation energy indicates that Li can insert in TiF_3 rather than clustering. The formation energy is lower than that of some typical anode materials, such as Nb_2C (−0.02 eV per Li).[51] In this Li concentration, the TiF_3 lattice undergoes tensile strains of about 6.7% in the x- and y-directions and 2.3% in the z-direction, which are much smaller than the volume expansion of Si (310%) and Sn (260%) upon lithium insertion.[52] We therefore took the stoichiometry of $LiTiF_3$ as the maximum Li capacity in the TiF_3 anode. The maximum theoretical capacities (C) of Li atom can be calculated by $C = x_{max}F/M_{TiF_3}$, where x_{max} is the maximum fraction of Li in Li_xTiF_3, F represents the Faraday constant (26.8 A h mol^{-1}), and M_{TiF_3} is the atomic mass of TiF_3 (104.86 g mol^{-1}). The maximum capacity is evaluated to be 256 mA h g^{-1}. The capacity is comparable to those of the nonmagnetic electrode materials, TiO_2 polymorphs (200 mA h g^{-1}),[53] GeS (256 mA h g^{-1}),[16] and MoS_2/graphene (338 mA h g^{-1}).[10]

Because the charge/discharge processes of TiF_3 follow the half-cell reaction *vs.* Li/Li^+: $Li_{1-x}TiF_3 + xLi + xe^- \leftrightarrow Li_xTiF_3$, the average open-circuit voltage (OCV) for Li intercalation can therefore be evaluated from the energy difference based on the following equation:

$$V_{ave} = -\frac{E[Li_{x_2}TiF_3] - E[Li_{x_1}TiF_3] - (x_2 - x_1)E_{Li}}{(x_2 - x_1)e}$$

where $E[Li_xTiF_3]$ is the total energy of the bulk TiF_3 with inserted Li atoms, E_{Li} is the energy of bulk Li crystal, and x_1 and x_2 represent the concentrations of Li atoms intercalated in bulk TiF_3. Therefore, the average open-circuit voltage is 0.08 V. The average open-circuit voltage in TiF_3 is much lower than those of TiO_2 (1.5 V)[53] and Cu_3N (0.38 V)[33] and comparable to that of graphene (0.10 V).[7] The lower the anodal open-circuit voltage, the higher the output voltage of the battery, which is beneficial to the application of battery.

We evaluated the energy density (ε_M) of the Li-ion spin battery by taking the effects of cathode into account using the equation $\varepsilon_M = -nFE/\sum M_i$, where n is the amount of electron transfer, F is the Faraday constant, E is equilibrium potential, and M_i is the molar mass of anode and cathode materials. The cathode material ($LiCoO_2$) used in LIBs has the average voltage of 3.8 V and the capacity of 140 mA h g^{-1}.[54] To match with the cathode, the mass ratio between the anode and the cathode was taken as 0.547, which gave the energy density of 337 mW h g^{-1}. This value is larger than the energy density (265 mW h g^{-1}) achieved recently in the Li-ion battery.[54] In addition, the half-metallic anode filters the current into a single spin channel without needing half-metallic features of the cathode, provided that the spin is preserved in the whole circuit.

D. Thermal stability of the ferromagnetism of the Li-inserted TiF_3 crystal

We investigated the thermal stability of ferromagnetism of the TiF_3 crystal with inserted Li ions using the Ising model. Without external field, the Hamiltonian of the Ising model is written as $\hat{H} = -J_0 \sum_{ij} \hat{m}_i \hat{m}_j$, where $\hat{m}_i$ and $\hat{m}_j$ are the magnetic moments at the sites i and j, respectively, and J_0 is the exchange parameter. For the TiF_3 crystal, the value of J_0 can be determined using the formula $J_0 = \Delta E/16m^2$, where ΔE is the energy difference between ferromagnetic (FM) and antiferromagnetic (AFM) states, and $\Delta E = E_{FM} - E_{AFM}$. For $Li_{0.125}TiF_3$, J_0 was evaluated to be 4.5 meV, and the possible values of $\hat{m}$ were taken as -1 and 1. Based on these parameters, we investigated the thermal stability of the FM states using Monte Carlo (MC) simulations. We employed a $30 \times 30 \times 30$ supercell containing 2.7×10^4 local magnetic moments. The simulations lasted for 1×10^8 loops. In each loop, the spins on all the sites in the supercell changed according to the spin states of Ti, yielding 2.7×10^{12} trials during the simulations. The spin was changed when $\Delta H \leq 0$ or random number $x < \exp(\Delta H/kT)$ is satisfied, where ΔH is the energy difference between the reversed spin state and initial state. The total energy of the system at each state was calculated using the Ising model. We obtained the magnetic moments as a function of temperature, as shown in Fig. 4. It can be observed that the magnetic moments per unit cell rapidly fall to 0.0 μ_B when the temperature is greater than 238 K, which indicates that the system undergoes a transition from ferromagnetic configuration (FM) to a paramagnetic configuration (PM) with an increase in temperature. To clarify the ferromagnetic–paramagnetic transition, we calculated the heat capacity (C_V) of the system using the expression: $C_V = \lim_{\Delta T \to 0} \frac{\Delta E_T}{\Delta T}$, where ΔE_T is the change in the total energy of the system as the temperature is increased from T to $T + \Delta T$. The calculated C_V as a function of temperature is shown in the inset of Fig. 4. It is obvious that the Curie temperature (T_C) is 238 K, and the ferromagnetic–paramagnetic transition is a second order transition. We also evaluated the Curie temperatures of Li_xTiF_3 ($x = 0.25$, 0.5 and 1.0) using the same strategy and found that they are 141 K, 85 K and 97 K, respectively. These Curie temperatures are higher than the temperature of liquid nitrogen (77 K) and can thus be easily achieved in experiments.

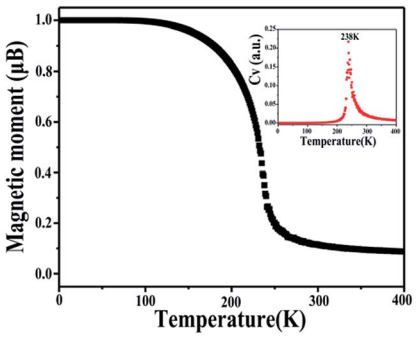

Fig. 4 Variation of the magnetic moment as the temperature. The temperature dependent heat capacity is plotted in the inset of the figure.

Finally, we should state that we only show an idea of Li-ion spin batteries in this work. Some complicated processes, such as spin injection and possible substitution reaction between Li and Ti atoms, have not been taken into account, and they are the objectives of the following studies.

Conclusions

Using first-principles calculations, we propose a potential half-metallic anode material for LIBs where the intrinsic electron spins are involved. We demonstrated that the TiF_3 crystal has not only robust ferromagnetism against Li insertion but also low energy barrier (0.16–0.37 eV) for Li diffusion. The Li storage capacity (256 mA h g^{-1}) and the average electrode potential (0.08 V) are comparable to those of the nonmagnetic anode materials. The combination of the half-metal with LIBs may offer a promising solution for long-desired spin batteries in spintronics.

Conflicts of interest

There are no conflicts of interest to declare.

Acknowledgements

This study is supported by the National Natural Science Foundation of China (No. 21433006, 11774201), the 111 project (No. B13029), the National Key Research and Development Program of China grant 2016YFA0301200, and the National Super Computing Centre in Jinan.

References

1 M. Armand and J.-M. Tarascon, *Nature*, 2008, **451**, 652–657.
2 Y. Idota, T. Kubota, A. Matsufuji, Y. Maekawa and T. Miyasaka, *Science*, 1997, **276**, 1395–1397.
3 T. S. Zhao, Q. Wang and P. Jena, *ACS Energy Lett.*, 2016, **1**, 202–208.
4 N. Nitta, F. X. Wu, J. T. Lee and G. Yushin, *Mater. Today*, 2015, **18**, 252–264.
5 J.-M. Tarascon and M. Armand, *Nature*, 2001, **414**, 359–367.
6 D. P. Dubal, O. Ayyad, V. Ruiz and P. Gómez-Romero, *Chem. Soc. Rev.*, 2015, **44**, 1777–1790.
7 J. R. Dahn, *Phys. Rev. B: Condens. Matter Mater. Phys.*, 1991, **44**, 9170–9177.
8 C. Uthaisar and V. Barone, *Nano Lett.*, 2010, **10**, 2838–2842.
9 Q. Tang, Z. Zhou and Z. Chen, *Nanoscale*, 2013, **5**, 4541–4583.
10 L. David, R. Bhandavat and G. Singh, *ACS Nano*, 2014, **8**, 1759–1770.
11 D. Er, J. Li, M. Naguib, Y. Gogotsi and V. B. Shenoy, *ACS Appl. Mater. Interfaces*, 2014, **6**, 11173–11179.
12 J. Hu, B. Xu, S. A. Yang, S. Guan, C. Ouyang and Y. Yao, *ACS Appl. Mater. Interfaces*, 2015, **7**, 24016–24022.
13 Q. Tang, Z. Zhou and P. Shen, *J. Am. Chem. Soc.*, 2012, **134**, 16909–16916.
14 W. Li, Y. Yang, G. Zhang and Y.-W. Zhang, *Nano Lett.*, 2015, **15**, 1691–1697.
15 J. Wu, D. Wang, H. Liu, W.-M. Lau and L.-M. Liu, *RSC Adv.*, 2015, **5**, 21455–21463.
16 F. Li, Y. Qu and M. Zhao, *J. Mater. Chem. A*, 2016, **4**, 8905–8912.
17 R. A. de Groot, F. M. Mueller, P. G. van Engen and K. H. J. Buschow, *Phys. Rev. Lett.*, 1983, **50**, 2024–2027.
18 W. E. Pickett and J. S. Moodera, *Phys. Today*, 2001, **54**, 39–44.
19 S. A. Wolf, D. D. Awschalom, R. A. Buhrman, J. M. Daughton, S. von Molnár, M. L. Roukes, A. Y. Chtchelkanova and D. M. Treger, *Science*, 2001, **294**, 1488–1495.
20 K. Schwar, *J. Phys. F: Met. Phys.*, 1986, **16**, 211–215.
21 J. E. Medvedeva, A. J. Freeman, X. Y. Cui, C. Stampfl and N. Newman, *Phys. Rev. Lett.*, 2005, **94**, 146602.
22 G. Y. Gao and K. L. Yao, *Appl. Phys. Lett.*, 2007, **91**, 082512.
23 L. Li, G. Lei, Q. Gao, J.-B. Deng and X.-R. Hu, *Mater. Res. Bull.*, 2015, **68**, 308–313.
24 E. Yan, *Phys. B*, 2012, **407**, 879–882.
25 H.-H. Xie, R.-Y. Ma, Q. Gao, L. Li and J.-B. Deng, *Chem. Phys. Lett.*, 2016, **661**, 89–93.
26 X. Dai, G. Liu, G. H. Fecher, C. Felser, Y. Li and H. Liu, *J. Appl. Phys.*, 2009, **105**, 07E901.
27 G. D. Liu, X. F. Dai, H. Y. Liu, J. L. Chen, Y. X. Li, G. Xiao and G. H. Wu, *Phys. Rev. B: Condens. Matter Mater. Phys.*, 2008, **77**, 014424.
28 M. Benkabou, H. Rached, A. Abdellaoui, D. Rached, R. Khenata, M. H. Elahmar, B. Abidri, N. Benkhettou and S. Bin-Omran, *J. Alloys Compd.*, 2015, **647**, 276–286.
29 H.-H. Xie, Q. Gao, L. Li, G. Lei, G.-Y. Mao, X.-R. Hu and J.-B. Deng, *Comput. Mater. Sci.*, 2015, **103**, 52–55.
30 J.-H. Park, E. Vescovo, H.-J. Kim, C. Kwon, R. Ramesh and T. Venkatesan, *Nature*, 1998, **392**, 794–796.
31 V. P. Ehrlich and G. Pietzka, *Z. Anorg. Allg. Chem.*, 1954, **275**, 121–140.
32 A. Mogus-Milankovic, J. Ravez, J. P. Chaminade and P. Hagenmuller, *Mater. Res. Bull.*, 1985, **20**, 9–17.
33 J. Wang, F. Li, X. Liu, H. Zhou, X. Shao, Y. Qu and M. Zhao, *J. Mater. Chem. A*, 2017, **5**, 2328–2338.
34 M. V. Reddy, S. Madhavi, G. V. Subba Rao and B. V. R. Chowdari, *J. Power Sources*, 2006, **162**, 1312–1321.
35 P. Ehrlich, F. Plöger and G. Pietzka, *Z. Anorg. Allg. Chem.*, 1955, **282**, 19–23.
36 G. Kresse and J. Furthmuller, *Phys. Rev. B: Condens. Matter Mater. Phys.*, 1996, **54**, 11169–11186.
37 G. Kresse and D. Joubert, *Phys. Rev. B: Condens. Matter Mater. Phys.*, 1999, **59**, 1758–1775.
38 J. P. Perdew, K. Burkeand and Y. Wang, *Phys. Rev. B: Condens. Matter Mater. Phys.*, 1996, **54**, 16533–16539.
39 J. P. Perdew, K. Burke and M. Ernzerhof, *Phys. Rev. Lett.*, 1996, **77**, 3865–3868.
40 D. J. Chadi, *Phys. Rev. B: Solid State*, 1977, **16**, 1746–1747.
41 G. Henkelman, B. P. Uberuaga and H. Jónsson, *J. Chem. Phys.*, 2000, **113**, 9901–9904.
42 G. Henkelman and H. Jónsson, *J. Chem. Phys.*, 2000, **113**, 9978–9985.
43 N. Yamada, K. Maruya, Y. Yamaguchi, X. Cao and Y. Ninomiya, *Chem. Mater.*, 2015, **27**, 8076–8083.
44 Y. Kim, B. J. Wieder, C. L. Kane and A. M. Rappe, *Phys. Rev. Lett.*, 2015, **115**, 036806.
45 F. Gulo, A. Simon, J. Kohler and R. K. Kremer, *Angew. Chem., Int. Ed.*, 2004, **43**, 2032–2034.
46 J. B. Goodenough, *Phys. Rev.*, 1955, **100**, 564–573.
47 J. B. Goodenough, *J. Phys. Chem. Solids*, 1958, **6**, 287–297.
48 J. Kanamori, *J. Phys. Chem. Solids*, 1959, **10**, 87–98.
49 V. V. Kulish, O. I. Malyi, M.-F. Ng, P. Wu and Z. Chen, *RSC Adv.*, 2013, **3**, 4231–4236.
50 S. Zhao, W. Kang and J. Xue, *J. Mater. Chem. A*, 2014, **2**, 19046–19052.
51 J. Hu, B. Xu, C. Ouyang, Y. Zhang and S. A. Yang, *RSC Adv.*, 2016, **6**, 27467–27474.
52 L. Y. Beaulieu, K. W. Eberman, R. L. Turner, L. J. Krause and J. R. Dahn, *Electrochem. Solid-State Lett.*, 2001, **4**, A137–A140.
53 Z. Yang, D. Choi, S. Kerisit, K. M. Rosso, D. Wang, J. Zhang, G. Graff and J. Liu, *J. Power Sources*, 2009, **192**, 588–598.
54 J. Wu, P. Liu, Y. Hu and H. Li, *Energy Storage Sci. Technol.*, 2016, **5**, 443–453.

